Mössbauer Studies of Lattice Dynamics, Fine and Hyperfine Structure of Divalent Fe^{57} in FeF$_2$*

D. P. JOHNSON

Advanced Materials Research and Development Laboratory, Pratt and Whitney Aircraft, Middletown, Connecticut 06458

AND

R. INGALLS

Physics Department, University of Washington, Seattle, Washington 98105

(Received 24 September 1969)

Mössbauer studies of the isomer shift, recoil-free fraction, and quadrupole splitting for Fe^{57} in FeF$_2$ between 80 and 300°K are reported. The temperature dependence of the isomer shift and recoil-free fraction are well explained within the harmonic approximation. The ascertained sum of the microscopic force constants acting on the Fe^{++} ion is $K = (1.24 \pm 0.07) \times 10^5$ dyn/cm. The weighted frequency average associated with the classical mean-square displacement of the Fe^{57} is $\langle 1/\omega^2 \rangle^{-\frac{1}{2}} = (2.08 \pm 0.05) \times 10^{13}$ sec^{-1}. Analysis of the quadrupole splitting, coupled with an analysis of the magnetic behavior by Lines, leads to a reassessment of the measurable effects of covalency upon the crystal-field, spin-orbit, and hyperfine interaction. The spin-orbit coupling parameter is estimated to be $\lambda = -85$ cm^{-1}. Using this value for the spin-orbit coupling parameter, the resulting crystal-field splitting of the $^5T_2$ orbital levels which describe the temperature dependence of the quadrupole splitting are $\Delta_1 = 780 \pm 40$ cm^{-1} and $\Delta_2 = 930 \pm 70$ cm^{-1}. The $\langle r^{-3} \rangle_{eff} = 3.0 \pm 0.3$ a_0^{-3} for the d electrons and the contact contribution to the internal field at 4.2°K is $H_c = -518 \pm 25$ kOe.

I. INTRODUCTION

IN this paper we report precision measurements of the isomer shift and Mössbauer fraction between 80 and 300°K for divalent Fe^{57} in FeF$_2$ (Secs. III A and III B).[1] These measurements follow a similar study of the same ion in FeCl$_2$ where the influence of low-temperature anharmonicity was clearly seen.[2] Here we find that the decreased nearest-neighbor distance prohibits such an effect.

We also report refined measurements of the nuclear quadrupole splitting of Fe^{57m} between 80 and 300°K (Sec. III C). Because of its relatively low value together with relatively flat temperature dependence, this splitting has been the object of considerable interest.[3-7] While a recent investigation by Ganiel and Shtrikman[8] has aided our understanding of the role of the crystal-field splitting of the Fe^{2+} ion, the relative importance of spin-orbit coupling, lattice electric-field gradient (EFG), and covalency have not previously been considered quantitatively. We do so here by making a direct calculation of the lattice EFG (Sec. III E) and a careful study of the sensitivity of the results to the spin-orbit parameter making extensive use of a recent re-determination of the spin-Hamiltonian parameters by Lines.[9] We also arrive at estimates for the hyperfine parameters,

$\langle r^{-3} \rangle_{eff}$ for the $3d$ electrons, and the contact contribution to the magnetic field at the Fe^{57} nucleus (Sec. III D). In addition we examine the ionic contributions to the crystal-field splittings of the Fe^{2+} ion (Sec. III F) utilizing the lattice-sum calculation of the lattice EFG and higher potential derivatives.

II. EXPERIMENTAL METHOD

A. Apparatus

The Mössbauer spectrometer used in measuring the velocity spectrum of FeF$_2$ is the same as previously described[2]. The velocity was calibrated to 0.6% by measuring the absorption spectra of a high-purity unenriched iron absorber.[10] The experimental line width of the 0.0006-cm-thick iron absorber versus a Cu(Co^{57}) source was found to be (0.202 ± 0.003) mm/sec indicating a thickness-corrected line width of (0.196 ± 0.003) mm/sec.

The stationary FeF$_2$ absorbers were mounted in a variable-temperature transmission cryostat[11] in which the absorber could be held for several days within 0.2°K of any desired temperature between 4 and 400°K. A clamping mechanism was developed which introduced no detectable instrumental broadening when the absorber was studied at low temperatures.[12]

B. Absorber Preparation

The samples studied in this work consisted of several unenriched powdered absorbers of anhydrous ferrous

* Supported in part by National Aeronautics and Space Administration.

[1] A preliminary report of this phase of the work is given by D. P. Johnson and J. G. Dash, Bull. Am. Phys. Soc. **12**, 901 (1967).

[2] D. P. Johnson and J. G. Dash, Phys. Rev. **172**, 983 (1968).

[3] G. K. Wertheim, Phys. Rev. **121**, 63 (1961).

[4] A. Abragam and F. Boutron, Compt. Rend. **252**, 2404 (1961).

[5] R. Ingalls, Phys. Rev. **133**, A787 (1964).

[6] A. Okiji and J. Kanamori, J. Phys. Soc. Japan **19**, 908 (1964).

[7] G. K. Wertheim and D. N. E. Buchanan, Phys. Rev. **161**, 478 (1967).

[8] U. Ganiel and S. Shtrikman, Phys. Rev. **177**, 503 (1969).

[9] M. E. Lines, Phys. Rev. **156**, 543 (1967).

[10] R. S. Preston, S. S. Hanna, and J. Herberle, Phys. Rev. **128**, 2207 (1962).

[11] D. P. Johnson, Ph.D. thesis, University of Washington, 1967 (unpublished).

[12] D. P. Johnson, G. A. Erickson, and J. G. Dash, Rev. Sci. Instr. **39**, 420 (1968).
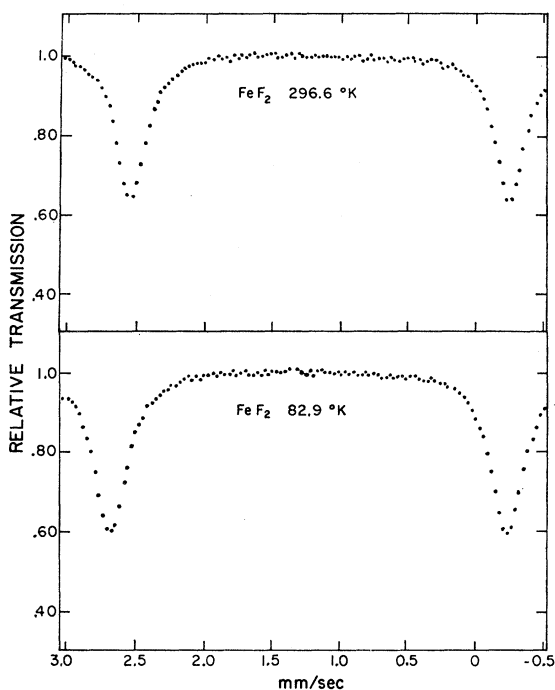
FIG. 1. Typical Mössbauer spectra reported in this work. Positive velocity corresponds to the source approaching the absorber.

fluoride prepared in a similar manner to that described in Ref. 2. Since FeF_2 is somewhat deliquescent, special care was taken to prevent water vapor from coming into contact with the powder. After the mounting procedure, the amount of hydration which occurred was checked by chemical analysis of similar samples and by examination of the Mössbauer spectra. If particular care is not taken in avoiding contact with the water vapor, a slight broadening of the high-velocity line is observed in the FeF_2 spectra associated with the contamination of the anhydrous FeF_2 powder with small amounts of hydrous FeF_2. This contamination will produce small errors by decreasing the quadrupole splitting and isomer shift. The spectra reported here are apparently free from this contamination.

The thickness uniformity was checked by measuring the transmission of 14-keV γ radiation through many different regions of the absorber, indicating that the long-range variation in thickness of these absorbers is a few percent. A FeF_2 absorber similar to those reported here was taken apart and examined under a microscope. The average microscopic variation was found to be less than ± 5 μ. The uncertainty in recoil-free fraction resulting from the variation in thickness is approximately 2%.

The absorbers had an average Fe^{57} thickness ranging from 0.255 to 0.561 mg/cm^2, assuming a natural relative abundance of Fe^{57} of 0.0219.[13] Background corrections were made in a similar manner to that described in Ref. 2. No small-angle inelastic scattering was observed.

Figure 1 is a plot of the velocity spectrum of the 0.255-mg/cm^2 sample at 269.4 and 82.9°K. The thickness-corrected experimental line widths are essentially equal to the natural width of 0.194 mm/sec,[14] which indicates that there is very little variation in chemical environment of the ferrous ions. The corrected line width at room temperature is 0.191 ± 0.005 mm/sec and at 83°K is 0.197 ± 0.005 mm/sec.

III. RESULTS AND DISCUSSION

A. Isomer Shift

The experimental velocity shift, or isomer shift,[15] of the FeF_2 absorber versus a room-temperature source can be written as[2]

$$\delta = \delta_0 - \langle v^2 \rangle_T / 2c,\qquad(1)$$

where δ_0 is the sum of the chemical shift and the constant second-order Doppler shift of the $Cu(Co^{57})$ source, $\langle v^2 \rangle_T$ is the mean-square velocity of the absorbing nuclei at temperature T, and c is the speed of light. The weak temperature dependence of the chemical shift[16] is estimated from the volumetric dependence of the chemical shift of the ferrous ion[17] and the temperature dependence of the volume.

For a harmonic crystal in thermal equilibrium at high temperature, the mean-square velocity can be written as

$$\langle v^2 \rangle_T = \frac{kT}{m_{Fe}} \sum_{\alpha=1}^{3} \left[1 + \frac{K^{\alpha\alpha}}{12m_{Fe}} \left(\frac{h}{kT}\right)^2 + \cdots \right],\qquad(2)$$

where m_{Fe} is the mass of the Fe atom, $K^{\alpha\alpha}$ is the force constant for the Fe atom in the α direction, for displacement in the α direction, while all other atoms in the crystal are fixed at their equilibrium position.[18]

Figure 2 is a plot of the experimental shift of FeF_2 as a function of temperature. The solid curve represents a fit with $\delta_0 = (1.348 + 0.25 \times 10^{-4}T)$ mm/sec and the mean-square velocity given by Eq. (2) with

$$K = (K^{xx} + K^{yy} + K^{zz}) = (1.24 \pm 0.07) \times 10^5 \text{ dyn/cm.}$$

Because over this limited temperature range the thermal shift is dominated by a single-frequency moment, it can be fit to a Debye model with a characteristic temperature $\Theta_D = (349 \pm 9)°K$ or an Einstein model with a characteristic temperature $\Theta_E = (270 \pm 7)°K$. The effects of an uncertainty in the temperature dependence of the chemical shift can be indicated by noting that if it were independent of temperature, δ_0

[13] A. H. Wapstra, J. Inorg. Nucl. Chem. 3, 329 (1957).

[14] A. H. Muir, K. K. Ando, and H. M. Coogan, Mossbauer Effect Data Index, 1958–1965 (Interscience Publishers, Inc., New York, 1966).
[15] Following custom (Ref. 14) we here refer to the sum of the chemical shift and second-order Doppler shift as the isomer shift, although this term was originated to stand for the chemical shift.
[16] R. V. Pound, G. B. Benedek, and R. Drever, Phys. Rev. Letters 7, 405 (1961).
[17] R. Ingalls, C. J. Coston, G. Depasquali, H. G. Drickamer, and J. J. Pinajiam, J. Chem. Phys. 45, 1057 (1966).
[18] R. M. Housley and F. Hess, Phys. Rev. 146, 517 (1966).

would increase by less than 1% and the characteristic temperature would increase by less than 6%.

B. Mössbauer Fraction

Several features of the absorption spectra can be used to determine the recoil-free fraction (f') of an absorber. In this study, the thickness dependence of the linewidth,[19] the maximum intensity,[20] and the integrated intensity[2] are used. All techniques give the same value for f' within the uncertainty in the measurements. However, the integrated intensity was the primary characteristic used in determining f' because of the considerably smaller experimental error. If the anisotropy in the mean-square displacement is not too large and the interatomic forces are harmonic, the average Mössbauer fraction is given by

$$f_{av}' = \exp(-\langle x^2 \rangle_T / \lambda^2),\qquad(3)$$

where $\lambda^2 = 0.0188$ Å^2 is the reduced wavelength of the 14-keV γ rays and $\langle x^2 \rangle_T$ is the average mean-square displacement of the iron ion in the direction of the incident radiation.

$$\langle x^2 \rangle_T = kT\left[\frac{1}{K'} + \frac{1}{12m_{Fe}}\left(\frac{h}{kT}\right)^2 + \cdots\right].\qquad(4)$$

The quantity K', which has dimensions of a force constant, is a complicated function of the microscopic force constants, independent of the masses of the atoms in the crystal.[21] It is related to a weighted mean frequency,[16] i.e.,

$$\frac{1}{K'} = \frac{1}{3m_{Fe}} \sum_{\alpha=1}^{3} \sum_i b_{i\alpha}^2/\omega_i^2,\qquad(5)$$

where $b_{i\alpha}$ is the amplitude of the Fe atom in the α direction resulting from the ith phonon, with frequency ω_i.
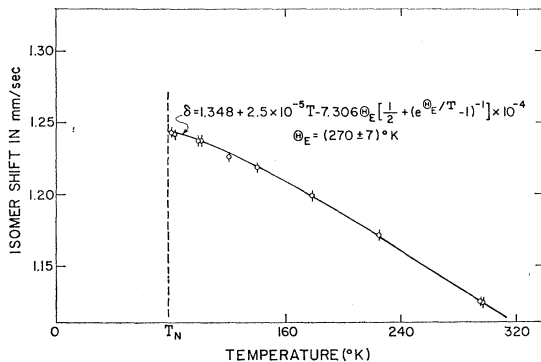

FIG. 2. Temperature dependence of the isomer shift compared with a calculation based upon the Einstein model.

[19] H. Frauenfelder *et al.*, Phys. Rev. **126**, 1065 (1962).
[20] S. Marqulies and J. R. Ehrman, Nucl. Instr. Methods **12**, 131 (1961).
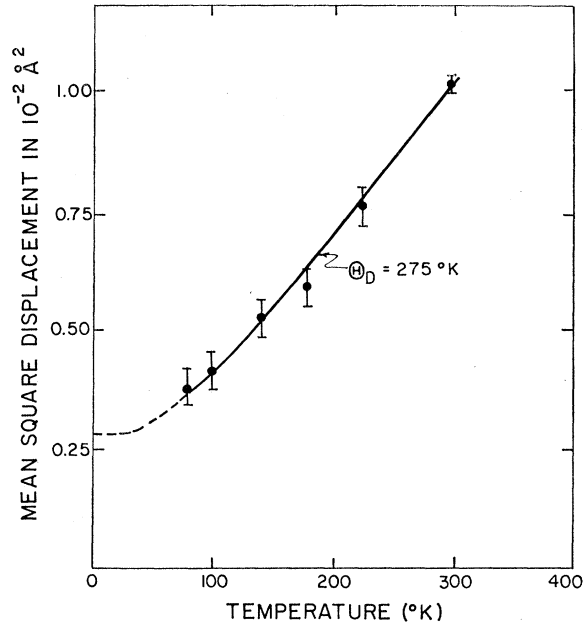[21] A. A. Maradudin and P. A. Flinn, Phys. Rev. **126**, 2059 (1962).

FIG. 3. Temperature dependence of the mean-square displacement compared with a calculation based upon the Debye model.

Figure 3 is a plot of the mean-square displacement ($-\lambda^2 \ln f_{av}'$) as a function of temperature. The solid line represents a theoretical fit with

$$(K'/m_{Fe})^{1/2} = (2.08 \pm 0.04) \times 10^{13} \text{ sec}^{-1}.$$

This frequency average corresponds to a Debye model with a characteristic temperature $\Theta_D = (275 \pm 5)°$K or an Einstein model with a characteristic temperature $\Theta_E = (159 \pm 3)°$K.

C. Quadrupole Splitting

The quadrupole splitting measured in this work is compared in Fig. 4 with other results[7,8] between 4 and 300°K. It is evident that the present data are in good agreement with Ref. 7 but somewhat higher than that in Ref. 8. A possible explanation for sample variation in the quadrupole splitting is given in Sec. II B.

The theory of quadrupole splittings in ferrous compounds in general,[5] and in FeF$_2$ in particular,[4,6,8] has already been given in sufficient detail to permit us to simply repeat the necessary results. As described briefly in the Introduction, our analysis here, and in Secs. III D and III F represents an extension of these earlier works.

One may express the quadrupole splitting in the following way[5]

$$\Delta E(T) = \Delta E_0 F(T).\qquad(6)$$

The bare quadrupole coupling constant ΔE_0 is defined as

$$\Delta E_0 = (2/7)\langle r^{-3} \rangle_{eff} e^2 Q,\qquad(7)$$

where $\langle r^{-3} \rangle_{eff}$ is an effective value for the $3d$ electrons on the ferrous ion including both covalency and antishielding effects, and Q is the quadrupole moment of
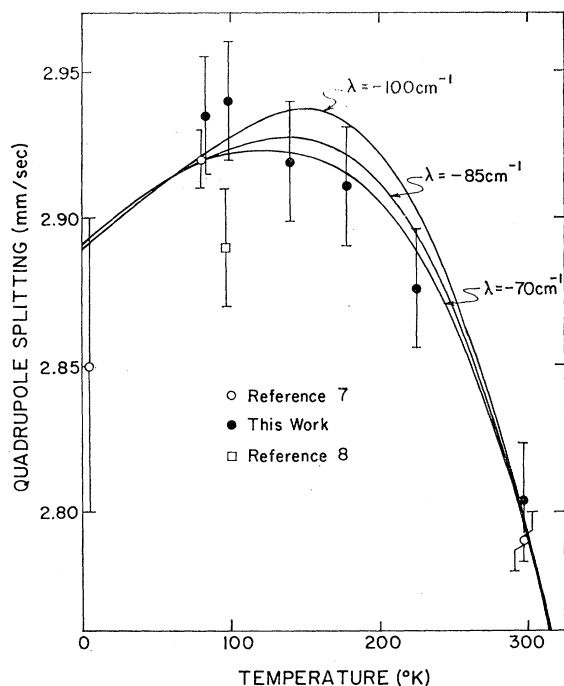
FIG. 4. Experimental quadrupole splittings between 4 and 300°K. The solid lines correspond to calculations using various values of the spin-orbit parameter λ (Sec. III E).

Fe^{57m}. The reduction factor $F(T)$ takes into account thermal averaging over crystal-field levels of the Fe^{2+} ion (Sec. III F and Figs. 5 and 7) and also includes the perturbation of the ion by magnetic exchange $(T<T_N)$ and spin-orbit coupling, as well as the EFG parameters due to the lattice.

The relevant low-lying $^5T_2$ orbitals for the Fe^{2+} ion are $|xz\rangle$, $|yz\rangle$, and $\alpha|x^2-y^2\rangle+\beta|3z^2-r^2\rangle$, where $\alpha^2+\beta^2=1$. The corresponding crystal-field levels, before further splitting, by magnetic or spin-orbit effects, are given by Δ_1 and Δ_2. For the choice of axes shown in Fig. 5, $\Delta_2>\Delta_1$ and $\alpha/\beta>0$ (see Sec. III F). Thus the factor F is regarded as a function of four adjustable parameters Δ_1, Δ_2, α, and λ (the spin-orbit parameter). Other parameters that would ordinarily appear are regarded as fixed. These include the higher orbital levels Δ_3 and Δ_4[22] and the lattice EFG parameters (Sec. III E). For the magnetic state we evaluate F at 4.2°K under the assumption that only the lowest spin-orbit level $(|S_x|=2)$ is occupied. In this instance the calculation is no longer sensitive to a magnetic-exchange parameter.

Since the value of ΔE_0 varies from compound to compound,[23] F is determined from the two quadrupole splitting ratios[7]

$$R_L \equiv F(4.2)/F(80) = 0.976 \pm 0.02,$$
$$R_H \equiv F(297)/F(80) = 0.956 \pm 0.008,$$
(8)

[22] G. D. Jones, Phys. Rev. 155, 259 (1967).
[23] R. Ingalls, Phys. Rev. 188, 1045 (1969).

and the total EFG asymmetry parameter[7]

$$\eta(4.2) = 0.40 \pm 0.02.$$

The quantities $F(80)$ and $F(297)$ are calculated by diagonalization of a 25×25 matrix,[5] while $\eta(4.2)$ and $F(4.2)$ are calculated using perturbation theory, taking into account the magnetically induced contributions.

The lattice EFG components are incorporated into the factor F in the manner prescribed in Ref. 5. For example, the Z component contribution to F is given by

$$-7(1-\gamma_\infty)V_{zz}/4e\langle r^{-3}\rangle_{eff},$$

where $(1-\gamma_\infty) \doteq 12$ is the antishielding factor[5] and $\langle r^{-3}\rangle_{eff} \doteq 0.04(\lambda/\lambda_0)a_0^{-3}$. The latter expression assumes that $\langle r^{-3}\rangle_{eff}$ is proportional to the spin-orbit parameter and a recent result based on the quadrupole coupling in $FeSiF_e \cdot 6H_2O$ which suggests that[23] $\langle r^{-3}\rangle_{eff} \doteq 4.0a_0^{-3}$ for $\lambda=\lambda_0=-100$ cm^{-1}. The uncertainties in $1-\gamma_\infty$ and $\langle r^{-3}\rangle_{eff}$ are unimportant here since the antishielded lattice EFG contributions are an order of magnitude less than the direct contribution from the $3d$ electrons on the ferrous ion. The estimate of the lattice EFG tensor used in this analysis is given in Sec. III E and Table I.

D. Fine and Hyperfine Parameters

The parameters Δ_1, Δ_2, λ, and β are determined by first fixing λ and then determining the three unknowns, Δ_1, Δ_2, and β, which yield the three experimentally known parameters R_H, R_L, and $\eta(4.2)$ [Eq. (8)].[24] The same procedure is repeated for several values of λ. Once the four parameters are chosen, $F(T)$ and then ΔE_0 can be determined. In Fig. 4, the variation of the quadrupole splitting with the spin-orbit parameter, subject to $\eta=0.40$, $R_L=0.990$, and $R_H=0.956$, is shown. The temperature dependence of the quadrupole splitting favor a $|\lambda| \lesssim 85$ cm^{-1}.

The same four parameters are used to calculate the spin-Hamiltonian constants D, E, $g_{||}$, and $g_\perp$ by perturbation theory,[6,8,9] including the uncertainties in D and E due to spin-spin coupling[6] (0 to 1 cm^{-1}) and uncertainties in $g_{||}$ and $g_\perp$ due to an orbital-reduction
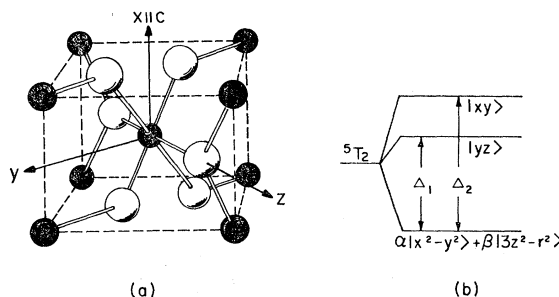

FIG. 5. Coordinate axes (a) and $^5T_2$ energy level scheme (b) used in this work.

factor[9] (1.0 to 0.8). These calculated spin-Hamiltonian constants are shown in Fig. 6 along with the value for these parameters from an extensive analysis by Lines[9] of such experimental quantities as sublattice spin, susceptibility, antiferromagnetic-resonance frequency, crystal-field anisotropy, and Néel temperature. These results favor a $|\lambda| \doteq 85$ cm^{-1}.

A major experimental uncertainty is the factor R_L. If this ratio was decreased below 0.990 to the value given in Eq. (8), the resulting fine-structure parameter would favor an even smaller value of $|\lambda|$. From the finding described above we adopt a value for $\lambda = -85$ cm^{-1}. This magnitude, we believe, represents something approaching an upper limit despite recent conclusions to the contrary.[25]

For $\lambda = -85$ cm^{-1}, the value of the remaining three parameters are $\Delta_1 = 780 \pm 40$ cm^{-1}, $\Delta_2 = 930 \pm 70$ cm^{-1}, and $\beta = 0.084 \pm 0.008$, where the errors reflect both the uncertainties in λ and the quadrupole data itself. These values are in reasonable agreement with the analysis of Ganiel and Shtrikman[8] and also give equally good agreement with their high-temperature data. The splitting of the orbitals due to spin-orbit and magnetic perturbation would result in an increase in the average energy separation between the occupied orbitals and the $|xz\rangle$ orbitals above that given by Δ_2. This would tend toward a far-infrared absorption in agreement with the experimental value[25] of 1115 cm^{-1}.

With the above value for the crystal-field parameters, $F(80) = 0.84$. The lattice electric-field reduction is approximately 10% and the spin-orbit reduction is approximately 6%. From Eq. (6),

$$\Delta E_0 = \Delta E(80)/F(80) = 3.5 \pm 0.1 \text{ mm/sec.}$$

The quadrupole moment Q can be eliminated from ΔE_0 by using the following results for $FeSiF_6 \cdot 6H_2O$: $\langle r^{-3}\rangle_{eff} = 3.5a_0^{-3}$ and $\Delta E_0 = 4.1$ mm/sec.[23] From Eq. (7) one obtains for FeF_2

$$\langle r^{-3}\rangle_{eff} = 3.0 \pm 0.3 a_0^{-3}.$$

Using perturbation theory,[4,6] and the above values for Δ_1, Δ_2, λ, β, and $\langle r^{-3}\rangle_{eff}$, the dipole and orbital con-

TABLE I. The calculated lattice-electric-field gradient at the iron lattice site in FeF_2 assuming the effective charge on the iron is $+1.6e$. The point-ion contribution is calculated with only point charges at the lattice sites. The total electric field gradient is calculated with a point charge at the iron lattice sites and two point charges near the fluoride lattice sites. The difference is the contribution from the induced polarization of the fluoride ion (choice of axes is given in Fig. 5).

	Point-ion contribution	Polarization contribution	Total (10^{15} V/cm^2)
$V_{zz} =$	-13.2	-4.8	$= -18.0$
$V_{yy} =$	12.2	$+0.4$	$= 12.6$
$V_{xx} =$	1.0	$+4.4$	$= 5.4$

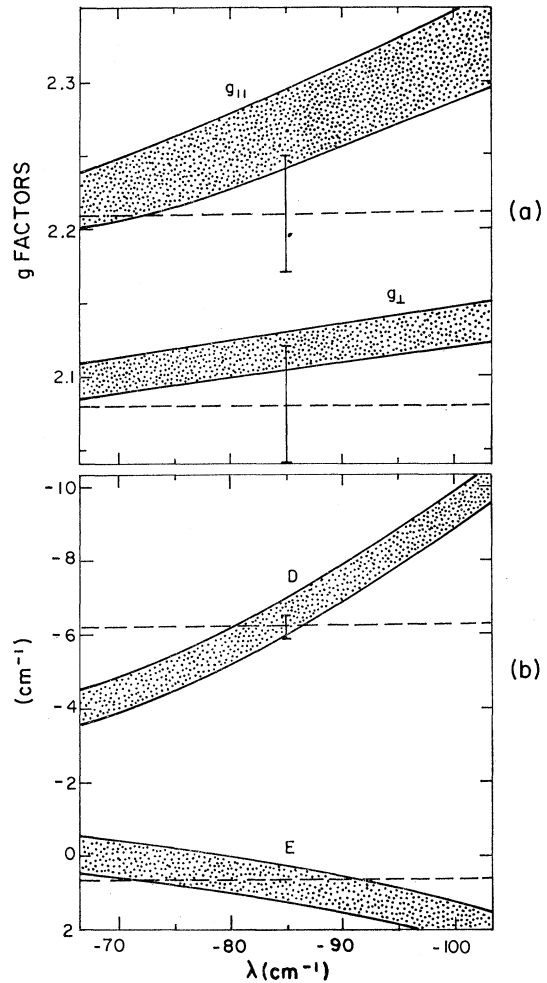[25] J. W. Stout, M. I. Stienfield, and M. Yuzuri, J. Appl. Phys. 39, 1141 (1968).

FIG. 6. Dependence of the spin-Hamiltonian parameters upon the spin-orbit constant λ. The shaded areas correspond to the parameters Δ_1, Δ_2, and β obtained from fitting the Mössbauer data. The lower bounds of each area for the g factors (a), are obtained with an orbital reduction factor of 0.85. The lower bounds for D and E (b) are obtained by adding 1 cm^{-1} to possibly account for spin-spin coupling. The dashed lines and bars correspond to an independent analysis by Lines (Ref. 9), with the error in $g_{\parallel}$ assumed equal to that reported for $g_{\perp}$.

tributions to the hyperfine magnetic field at 4.2°K can be calculated. The results are

$$H_{dipole} = -26 \pm 3 \text{ kOe},$$

$$H_{orbital} = 215 \pm 20 \text{ kOe}.$$

Since the measured value for the internal field is[7] $H_{int} = H_c + H_{dipole} + H_{orbital} = -329$ kOe, this leads to a contact contribution of

$$H_c = -518 \pm 25 \text{ kOe}.$$

The latter is to be compared with the theoretical calculation for the free ion,[26] $H_c = -550$ kOe. Values

[26] A. J. Freeman and R. E. Watson, Phys. Rev. 131, 2566 (1963).

TABLE II. The calculated lattice fourth derivative of the potential at the iron lattice site in FeF_2 assuming the effective charge on the iron is $+1.6e$ (choice of axes is given in Fig. 5).

	Point-ion contribution	Polarization contribution	Total $(10^{33}$ $V/cm^4)$
$d^4V/dz^4 =$	-2.4	-0.1	$= -2.5$
$d^4V/dy^4 =$	0.6	-0.1	$= 0.5$
$d^4V/dx^4 =$	0.1	$+0.3$	$= 0.4$

for other ionic compounds range from -420 to -500 kOe.[27–30]

The above results give some of the quantitative effects of covalency upon such factors at λ, $\langle r^{-3}\rangle_{eff}$, and H_c.

E. Lattice EFG Tensor and Higher Spatial Derivatives

An estimate of the components, $V_{\alpha\alpha} = \partial^2 V/\partial X_\alpha{}^2$, of the lattice EFG at the iron site and also the fourth derivatives, $V_{\alpha\alpha\alpha\alpha} = \partial^4 V/\partial X_\alpha{}^4$, of the lattice potential at the same site are obtained by considering point charges of $2Z$ and $-Z$ and including the effects of the induced dipole at the fluoride sites. The latter contributions, arise from the lack of inversion symmetry at the fluoride site and the polarizability of the fluoride ion.

The electric field, EFG, and higher derivatives of the lattice potential are calculated in the following manner: The potential resulting from a set of unit positive charges arranged in a tetragonal array and a uniform negative charge density of such a value that the net charge per unit cell is zero, is evaluated at any point of interest by the Ewald method.[31,32] By numerically differentiating this potential, the spatial derivative of interest can be obtained. The contribution of each of the six tetragonal sublattices which make up FeF_2 can be evaluated by multiplying the above spatial derivative, evaluated at the appropriate point, by the charge associated with the particular sublattice. The total spatial derivative is then given by the sum of the individual contributions. Since the net charge in a unit cell is zero, the contribution from the various uniform charge densities will sum to zero.

In order to estimate the induced dipole moment on the fluoride ion and its effect on the spatial derivatives of the potential, a simple shell model[33] is used to describe the fluoride ion. The fluoride ion in FeF_2 is assumed to be similar to the fluoride ion in LiF or NaF. Hence, the shell charge is assumed to be $-2e$ and the force constant connecting the core to the shell is assumed to be $K = 12\times10^5$ dyn/cm. This compares to a shell charge of $-2.1e$ and $-1.9e$ and a shell force constant of 13×10^5

dyn/cm and 11×10^5 dyn/cm found for the fluoride ion in LiF and NaF, respectively.[34,35]

An iterative procedure is used to calculate the displacement of the shell with respect to the core of the fluoride ion and hence the position of the shell and core in the lattice. The electric field E resulting from the point ions is calculated at the fluoride lattice site in the manner described above. The electric field produces a displacement ΔX between the positive core and the center of the negative shell

$$\Delta X = (2-Z)eE/K. \qquad (9)$$

Outside the shell, the fluoride ion appears as two point charges of $-2e$ and $(2-Z)e$ separated by an amount ΔX with the center of mass of the $9+Z$ fluoride electrons at the lattice point associated with the fluoride ion. The next approximation of the electric field can be calculated in a manner similar to that described above, except one now must sum over ten tetragonal sublattices ($2Fe^{++}$, $4F^{--}$ shells, $4F^+$ cores). The correction to the electric field at the fluoride site due to the polarization of the other fluoride ions is small with the negative shell being attracted toward the nearest iron ion, $\Delta X = 0.022$ $Z(2-Z)$ Å.

Having determined the positions of the fluoride shell and core sublattices, additional spatial derivatives are obtained by summing the contributions from the ten sublattices. Table I shows the calculated lattice electric field gradient and Table II shows the calculated fourth derivative of the potential at the iron site assuming $Z = 0.8$. The choice of axes is given in Fig. 5.

F. Crystal-Field Splittings

It is of interest to make use of the potential derivatives in Sec. III E in order to estimate the ionic contribution to the crystal-field splittings Δ_1 through Δ_4. A Taylor's expansion of the perturbation due to the

TABLE III. Calculated ionic contributions to the crystal-field splittings of the Fe^{2+} ion in FeF_2 compared with measured crystal-field splittings (units of 10^3 cm^{-1}). Also listed is the parameter β characterizing the ground-state orbital, $\alpha|x^2 - y^2\rangle + \beta|3z^2 - r^2\rangle$. The large discrepancy between the measured and calculated splittings, Δ_3 and Δ_4, is attributed to large covalency effects in the cubic and other fourth-order terms.

	Direct measurement	Indirect measurement (Sec. III D)	Ionic crystal-field contribution (Sec. III F)
Δ_1	$\cdots$	0.78 ± 0.04	1.0
Δ_2	1.1^a	0.93 ± 0.07	1.3
Δ_3	5.5^b	$\cdots$	1.3
Δ_4	9.0^b	$\cdots$	3.0
β	$\cdots$	0.084 ± 0.008	0.083

^{a} See Ref. 25. ^{b} See Ref. 22.

[27] C. E. Johnson, Proc. Phys. Soc. (London) **92**, 748 (1967).
[28] K. Ono, A. Ito, and T. Fujita, J. Phys. Soc. Japan **19**, 2119 (1964).
[29] J. D. Siegwarth, Phys. Rev. **155**, 285 (1967).
[30] H. N. Ok and J. G. Mullen, Phys. Rev. **168**, 563 (1968).
[31] P. P. Ewald, Ann. Physik **64**, 253 (1921).
[32] The authors would like to thank J. W. D. Connolly for calculating the Ewald sums.
[33] B. J. Dick, Jr., and A. W. Overhauser, Phys. Rev. **112**, 90 (1958).

[34] G. Dolling, H. G. Smith, R. M. Nicklow, Pr. R. Vijayaraghavan, and M. K. Wilkinson, Phys. Rev. **168**, 970 (1968).
[35] W. J. L. Buyers, Phys. Rev. **153**, 923 (1967).

external charges gives:

$$U(\mathbf{r}) = -eV(\mathbf{r})$$

$$= -e\Big[V(0) + \tfrac{1}{2} \sum_{\alpha,\beta=1}^{3} x_\alpha x_\beta V_{\alpha\beta}$$

$$+ \tfrac{1}{4} \sum_{\alpha,\beta=1}^{3} x_\alpha x_\beta x_\gamma x_\delta V_{\alpha\beta\gamma\delta} + \cdots\Big], \quad (10)$$

where $V_{\alpha\beta}$ and $V_{\alpha\beta\gamma\delta}$ are spatial derivatives of the lattice potential. Separating this expression into second- and fourth-order terms leads to

$$U(\mathbf{r}) = -eV_0 + U_{c4} + U_{a2} + U_{a4} + U_{r2} + U_{r4},$$

where the terms are defined as follows:

cubic: $U_{c4} = -(1/5)D_4[Y_4^0 - (5/14)^{1/2}(Y_4^4 + Y_4^{-4})]$
$$\times [3V_{zzzz} - 4(V_{xxxx} + V_{yyyy})];$$

axial: $U_{a2} = -D_2 Y_2^0 V_{zz},$
$$U_{a4} = -(2/5)D_4 Y_4^0[V_{zzzz}$$
$$+ 2(V_{xxxx} + V_{yyyy})]; \quad (11)$$

rhombic: $U_{r2} = -1\sqrt{6}D_2(Y_2^2 + Y_2^{-2})(V_{xx} - V_{yy}),$

$$U_{r4} = (2/5)^{1/2}D_4(Y_4^2 + Y_4^{-2})(V_{xxxx} - V_{yyyy}),$$
where
$$D_l = \frac{er^l}{l!}\left(\frac{4\pi}{2b+1}\right)^{1/2}$$

and Y_l^m are the usual spherical harmonics.[36]

The qualitative effect of the above perturbations upon the ^5D state is shown in Fig. 7. Using the calculations in Tables I and II together with[37] $\langle r^2 \rangle = 1.39 a_0^2$ and $\langle r^4 \rangle = 4.50 a_0^4$ one arrives at the four energy separations listed, in Table III, for comparison with the direct measurements[21,24] and results of Sec. III D.

The calculated ionic splittings Δ_1 and Δ_2 are in fair agreement with those deduced from experiment. They arise mainly from large second-order terms, U_{a2} and U_{r2}, with the corresponding fourth-order terms an order of magnitude smaller, and making a negative contribution towards them. The calculated ionic splittings Δ_3 and Δ_4 are observed to be much too small and are dominated by large cubic and other fourth-order terms. As Hubbard et al.[38] point out, the ionic contribution to the cubic splitting generally seems to be
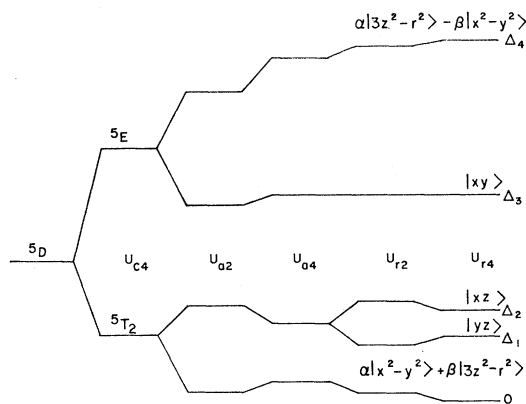

FIG. 7. Schematic diagram of the effect of the various crystal-field terms upon the ^5D splittings. Further splittings by spin-orbit and magnetic perturbations are not shown.

about half of the covalency contribution, but of the same magnitude. To our knowledge a modern treatment of the problem of covalency has not addressed itself to the axial and rhombic splittings in transition-metal complexes. Our findings suggest that covalency effects are decidedly more pronounced in the cubic and other fourth-order terms, since an enhancement of such terms would tend to bring all the splittings into closer agreement with experiment. The smaller covalent contributions to the splitting of the $^5T_2$ states as compared to the ^5E states might also be expected in view of the much smaller overlap between the iron d-orbitals and the fluoride ligand for $^5T_2$ states as opposed to the ^5E states.

The apparent agreement between the two values for β is probably an accident. This factor represents the coupling between the two orbitals, $|3z^2 - r^2\rangle$ and $|x^2 - y^2\rangle$ by the rhombic perturbations U_{r2} and U_{r4}. A large increase in the cubic separation between these states would tend to reduce β. However, such reduction could be countered by an increase in the term U_{r4} which adds to the effect of U_{r2} when coupling the above states.

In conclusion, it is striking how well FeF_2 exhibits all the expected effects of simple weak-crystal-field theory. Virtually every quantity associated with the $^5T_2$ states follows from relatively simple perturbation theory. It is hoped that a first-principles calculation, including covalency, can soon be made of the crystal-field splittings.

ACKNOWLEDGMENTS

---

[36] We have used the following relations to simplify (10):

$$\sum_{\alpha=1}^{3} V_{\alpha\alpha} = 0 \quad \text{and} \quad \sum_{\alpha=1}^{3} V_{\alpha\alpha\beta\beta} = 0.$$

In the principal-axis system, Fig. 5, terms like $V_{\alpha\beta}$ and $V_{\alpha\beta\gamma\gamma}$, etc., vanish for $\alpha \neq \beta$. Moreover, in this system, $V_{xxxx} = V_{yyyy} = -\tfrac{1}{4}V_{zzzz}$ for a regular octahedron, so that U_{a4} would vanish, as expected.

[37] R. Ingalls, Technical Report No. 2, Carnegie Institute of Technology, 1962 (unpublished).
[38] J. Hubbard, D. E. Rimmer, and F. R. A. Hopgood, Proc. Phys. Soc. (London) 88, 13 (1966).